



Enhanced Adsorption and Antimicrobial Activity of Fabricated Apocynaceae Leaf Waste Activated Carbon by Cobalt Ferrite Nanoparticles for Textile Effluent Treatment

V. Suba^{1,2} · G. Rathika¹ · E. Ranjith Kumar³ · M. Saravanabhavan² · Vishnu Nayak Badavath⁴ · K. S. Thangamani²

Received: 20 June 2018 / Accepted: 23 November 2018
© Springer Science+Business Media, LLC, part of Springer Nature 2019

Abstract

Novel nano composite (ALW/CoFe₂O₄) adsorbent was synthesized from Apocynaceae leaf waste activated carbon (ALW) in combination with CoFe₂O₄ by an auto combustion method for the removal of Reactive Red 141 dye and microorganisms against *S. aureus*, *E. coli* and *C. albicans*. The synthesized nano composite ALW/CoFe₂O₄ was characterized by SEM, EDX, BET, XRD, FTIR, TG & DSC and VSM. The results from these analytical techniques confirmed the aggregation of CoFe₂O₄ nano particles on the surface of ALW and VSM study showed its magnetic behavior. Subsequently, ALW/CoFe₂O₄ was adopted in batch mode adsorption studies by varying pH, adsorbent dosage, concentration and temperature. The adsorption efficiency was investigated under optimum conditions such as pH(6.5), adsorbent dosage (50 mg), contact time (70 min). The feasibility of adsorption was analyzed by fitting the data with pseudo first order, pseudo second order, Langmuir isotherm and Freundlich isotherm. The results showed that pseudo second order kinetics and Langmuir isotherm equation favour the adsorption of RR 141 on ALW/CoFe₂O₄. According to the thermodynamic study, it was very effective at higher temperatures and the thermodynamic parameters ΔG° , ΔH° and ΔS° were also evaluated for this adsorption. Furthermore, the antimicrobial activity of ALW/CoFe₂O₄ was tested by well diffusion method and compared with standard antibiotic. This ALW/CoFe₂O₄ exhibit good antimicrobial action with the zone of inhibition in the range of 10–17 mm. The synthesized nano composite (ALW/CoFe₂O₄) was evaluated for antimicrobial activity against (*Staphylococcus aureus*, *Escherichia coli* and *Candida albicans*), using well diffusion method and compared with standard antibacterial (Streptomycin) and antifungal (Amphotericin B). The antibacterial activity of ALW/CoFe₂O₄ against *S. aureus* (range between from 11.83 ± 0.23 mm to 17.5 ± 0.16 mm) and (range between *E. coli* 10.5 ± 0.40 to 17.0 ± 0.41 mm), while antifungistatic effect against *C. albicans* (range between 11.0 ± 0.24 to 17.6 ± 0.08), with different concentrations (100–500 mg) From the obtained results the antimicrobial activity of synthesized ALW/CoFe₂O₄ more or less same in the range between 11 and 17.56 mm of zone of inhibition.

Keywords Nano composite · Magnetic behaviour · Surface area · Adsorption · Water treatment · Antimicrobial activity

✉ G. Rathika
rathika_psg@yahoo.com

✉ E. Ranjith Kumar
ranjaueaswar@gmail.com

¹ Department of Chemistry, P.S.G College of Arts and Science, Coimbatore 641014, India

² Department of Chemistry, Dr. N.G.P. Institute of Technology, Coimbatore 641048, India

³ Department of Physics, Dr. N.G.P. Institute of Technology, Coimbatore 641048, India

⁴ Department of Microbiology, Faculty of Medicine, Chulalongkorn University, Bangkok 10330, Thailand

1 Introduction

One of the major sources of environmental problem is the disposal of toxic industrial effluents containing dyes into water bodies [1]. The rapid development of economy and industry result the discharge of colored waste water without reasonably processing which has a calamitous effect on environment and human health and affects the food cycle in water eco systems [2]. Treatment of hazardous industrial effluent is urgent to find an effective approach to deal with organic dyes of the dye-wastewater before discharging it into the environment because many dyes are usually stable and reduce light penetration and photosynthesis [3]. Different technologies have been developed to remove dyes from

effluent such as membrane separation, electro coagulation, precipitation, ion exchange, biosorption and adsorption [4]. Recently magnetic adsorption technology has been one of the promising technologies for dye sequestration by magnetic adsorption, extensively applied for treating waste water. This effluent treatment may include the synthesis of activated carbon (AC) from plant wastes as successful adsorbent for removal of organic and inorganic contaminants. However, during filtration, activated carbon requires high energy centrifugation and separation technologies to separate and retrieve [5]. To overcome the disadvantages of AC, the surface of AC is functionalized by the use of magnetic nano particles to increase the adsorption capacity and to separate easily from the aqueous solution.

In recent years, the most favorable nanotechnology is applied in various fields such as defense, electronics, storage media, environmental engineering and biomedical [6]. The magnetic nano particles result in unique functional applications because of their significant high surface area to volume ratio, physical and chemical properties than bulk counter parts [7]. Among the various nano particles, ferrite nano particles are of considerable interest because they show fundamental changes in structural and concomitant electronic rearrangements and significant dominance of the surface atoms [8]. In particular, cobalt ferrite particles are now attracted due to the presence of activating groups which attack organic compounds, high chemical stability, moderate magnetic saturation and easy separation [9]. The pollutant adsorption onto fabricated AC with spinel CoFe_2O_4 may be due to hydrogen bonding, surface complexation and electrostatic interaction. In this case, surface hydroxyl groups and surface charge are binding sites for various cationic and anionic species and they contribute to adsorption capacity [10].

In addition, untreated wastewater usually contains numerous pathogenic or disease causing microorganisms because of its ability to retain moisture. In the class of many microorganisms, *Escherichia coli* is a genus of gram-negative bacteria, rod shaped and non-spore forming bacteria and are pathogenic. They are the inhabitants of gastrointestinal tracts of warm-blooded animals [11]. *Staphylococcus aureus* is a gram-positive, round-shaped bacterium that is a member of the Firmicutes, and it is a member of the normal flora of the body, frequently found in the nose, respiratory tract, and on the skin. Further, *Candida species* affect nail, skin, and mucosal surfaces and cause the opportunistic yeast infection widely known as *Candidiasis*. Therefore, disinfection is also a part of treatment of wastewater containing many microorganisms which affect human health. Metal and metal oxides present in metal nano particles have greater resistance against microorganisms due to their stability at higher temperatures and pressures. Rokas Zalneravicius et al., reported antimicrobial activity of size dependent cobalt

ferrite nanoparticles against *S. Cerevisiae*, *C. parapsilosis*, *C. krusei* and *C. albicans* strains [12]. Noppakun Sanpo et al., has shown the biomedical applications of Transition metal-substituted cobalt ferrite nanoparticles. The substitution of transition metals strongly influence the antibacterial property of cobalt ferrite nanoparticles. Among the transition metals Cu, Zn, Cr, and Ni, Cu substituted nanoparticles have shown the most effective contact biocidal property [13]. A.H. Ashour et al., synthesized most potent Zn substituted cobalt ferrite nanoparticles and showed strong antimicrobial activity by gamma irradiation at 150 kGy which decreased the particle size of nanoparticles from 14.64 to 12.33 nm and elevated its antimicrobial activity against *S. aureus* (16.0 mm ZOI), *P.aeruginosa* (15.0 mm ZOI) and *C.albicans* (15.0 m ZOI) [14]. M.I.A.Abdel MAksoud et al., investigated bi-functional biosensor activity of Zn substituted cobalt ferrite nanoparticles to determine the drug Anagrelide-HCl (ANDH) in urine and serum samples and also antimicrobial potential against *Klebsiella pneumoniae* (28.0 mm ZOI), and multidrug-resistant bacteria *Enterococcus faecalis* (27.0 mm ZOI) and *Candida albicans* (18.0 mm ZOI) [15]. Moreover, Activated carbon (AC) has also been widely used for the removal of various infectious pollutants in wastewater because of its large surface area and high adsorption capacity. Antimicrobial Activity of Chemically modified Activated carbon prepared from *Tribulus terrestris* has been proved by Karthik and Saraswathy [16]. Kumar et al., employed activated Carbon impregnated with Ag, ZnO and Ag/ZnO nanoparticles as Antimicrobial Materials. They found the minimum inhibitory concentration (MIC) and minimum bactericidal concentration (MBC) of Ag/ZnO-AC nanohybrid against standard reference cultures with *E. coli* (0.20 mg/ml) and *S.aureus* (0.30 mg/ml) while MBC was found to be 0.35 mg/ml with *E. coli* and 0.6 mg/ml with *S.aureus* [17].

In this current work, the novel, cost effective pink flowered Apocynaceae leaf waste (ALW) activated carbon has been introduced. Nerium Oleander plant is evergreen shrub that grows up to the height of 4 m and bearing leaves all the year around. The leaves are long, linear-lanceolate, 10–15 cm in length with horizontal nerves. Then the surface of ALW activated carbon has been functionalized by magnetic cobalt ferrite (CoFe_2O_4) by an auto combustion method to improve the adsorption capacity of ALW for Reactive Red 141. The physico chemical and morphological characterization of AC and ALW/ CoFe_2O_4 were compared by taking SEM, XRD, EDAX, FT-IR, BET analysis, TG and DSC analytical techniques. The modified ALW/ CoFe_2O_4 has been utilized as an adsorbent for the removal of Reactive Red 141 from aqueous solution. Subsequently, their antimicrobial activities were tested against *S. aureus*, *E. coli* and *C.albicans*.

2 Materials and Methods

2.1 Materials

Apocynaceae leaf wastes were collected from highway regions of Coimbatore, India. Analytical grade of Cobalt nitrate, Ferric nitrate and Urea were purchased and used for the synthesis of ALW/CoFe₂O₄. A Reactive red 141 dye with molecular formula C₅₂H₂₆Cl₂N₁₄Na₈O₂₆S₈ and molecular weight 1774.19 was purchased from textile and design company. The stock solution of dye was made by dissolving it in double distilled water and the stock solution was further diluted to different concentrations of standard solution of 100 mg/L, 125 mg/L, 150 mg/L, 175 mg/L and 200 mg/L.

2.2 Methods

2.2.1 Preparation of ALW/CoFe₂O₄

Apocynaceae leaf wastes were washed thoroughly with distilled water to remove impurities and dried under sunlight for one month to remove all moisture present. The dried leaves were ground and impregnated with phosphoric acid for 24 h. The sample was then pyrolysed in a muffle furnace in absence of air at 600 °C for 2 h. After pyrolysis, the resulting sample was washed repeatedly to reach the pH of 6–7. This Apocynaceae leaf waste Activated Carbon (ALW) was dried in hot air oven and used for the synthesis of nano composite. An auto combustion method has been chosen to synthesize magnetic ALW/CoFe₂O₄. 1 mol of Co(NO₃)₂·6H₂O and 2 mol of Fe(NO₃)₃·9H₂O were dissolved in 50 mL of distilled water and 50% aqueous urea and 2 g of ALW were added to the above solution and then heated at 160 °C with constant stirring using magnetic stirrer for 1 h. On ignition in air at room temperature, the dried gel was burnt in a self propagating combustion, giving rise to the evolution of large amount of gases and producing a dry and loose powder.

2.2.2 Characterization of ALW/CoFe₂O₄

The surface morphology and composition of synthesized ALW/CoFe₂O₄ were investigated by Scanning electron microscope (JEOL Model—JSM 6390 LV) which was equipped with an energy dispersive X ray analyzer with magnification range of 30,000 and an accelerating voltage of 20 kV. The powder X ray diffraction pattern was performed using X-ray diffractometer (Shimadzu, XRD 6000) with a voltage of 40 kV and tube current of 30 mA using Cu cathode X-ray source ($\lambda = 0.1548$ nm) in the region of 2θ from 10° to 90°. The specific surface area and pore size distributions were characterized by Brunauer-Emmett-Teller (BET) method.

The magnetizable measurements were detected using a vibration sample magnetometer (Lakeshore VSM 7410) and recorded from – 15,000 Oe to 15,000 Oe at room temperature. The thermal stability and Differential Scanning Calorimetry were analyzed by thermo gravimetric analyzer (NETZSCH STA 449F3) with a heating rate of 10 °C/min. in the range of 25–600 °C under nitrogen flow. Infrared spectra of ALW/CoFe₂O₄ was obtained using Fourier Transform Infrared spectrometer (FT/IR-4600typeA, JASCO).

2.2.3 Batch Adsorption Studies

The adsorption of Reactive Red (RR141) from aqueous solution by ALW/CoFe₂O₄ was performed by examining different parameters like pH, contact time, initial dye concentration, composite dosage and temperature. The experimental studies were carried out by agitating 50 mL of aqueous RR141 with ALW/CoFe₂O₄ (50 mg) at different pH levels (3–12) for different time periods (5–90 min) at the temperature range (30–60 °C) at 200 rpm. After adsorption, the magnetic nano composite was separated by a magnet and the concentration of RR141 in a supernatant was measured by UV–Visible spectrophotometer. The percentage removal of RR141 was calculated using the following relationship,

$$\% \text{ Removal} = \frac{C_0 - C_e}{C_0} \times 100 \quad (1)$$

where C_0 and C_e are the initial and equilibrium concentration of RR141 respectively.

The adsorbed amounts of RR141 were calculated by the following equation

$$q = \frac{(C_0 - C_e) \times v}{m} \quad (2)$$

v is the volume of dye solution and m is the mass of adsorbent used.

To find the rate of adsorption on ALW/CoFe₂O₄, pseudo first order, pseudo second order kinetics were adopted for probable fitting of experimental data. The best fitted kinetic model for this adsorption system was identified by comparing the data obtained from experimental adsorption capacity [$q_e(\text{exp})$] and the calculated adsorption capacity [$q_e(\text{cal})$] and the higher correlation coefficient values (R^2). The linear equation for pseudo first order and pseudo second order kinetic models are

$$\log(q_e - q_t) = -\frac{k_1 t}{2.303} + \log q_e \quad (3)$$

$$\frac{t}{q_t} = \frac{1}{k_2 q_e^2} + \frac{t}{q_e} \quad (4)$$

where k_1 and k_2 are the pseudo first order and pseudo second order rate constants (min^{-1}), q_e and q_t are the amounts of RR141 adsorbed (mg/g) at equilibrium and at time t (min).

The adsorption isotherm equations play an important role in describing the interactive behavior between solutes and adsorbents and in determining the adsorption capacity of ALW/CoFe₂O₄. Langmuir and Freundlich isotherm equations have been taken to analyze the adsorption system. The linear form of Langmuir equation is represented by

$$\frac{C_e}{q_e} = \frac{1}{K_L q_m} + \frac{C_e}{q_m} \quad (5)$$

where C_e is the equilibrium concentration of RR141 (mg/L), q_e is the amount adsorbed at equilibrium (mg/g), q_m is maximum adsorption capacity (mg/g) and K_L is Langmuir coefficient and is related to energy of adsorption (L/mg). The linearity of the isotherm can also be used to predict whether the adsorption is favorable or unfavorable. The essential characteristics of Langmuir isotherm can be reflected by a dimensionless constant called equilibrium parameter R_L which is defined by

$$R_L = \frac{1}{1 + K_L C_0} \quad (6)$$

where C_0 is the initial concentration (mg/L) and R_L value implies the adsorption to be unfavorable ($R_L > 1$), Linear ($R_L = 1$), Favorable ($0 < R_L < 1$) or Irreversible ($R_L = 0$).

The empirical Freundlich isotherm equation based on sorption on to heterogeneous surface can be written as

$$\log q_e = \log K_F + \frac{1}{n} \log C_e \quad (7)$$

where K_F and $1/n$ are the constants which represent the adsorption capacity and adsorption intensity respectively and were obtained from intercept and slope of linear regression plot.

The nature of adsorption is confirmed by various thermodynamic parameters which provide information regarding energetic changes. The thermodynamic parameters such as standard free energy change (ΔG°), enthalpy change (ΔH°) and entropy change (ΔS°) were evaluated to verify the

feasibility and spontaneous nature of adsorption. The values were determined using the following Van't Hoff equation,

$$\Delta G^\circ = -RT \ln K \quad (8)$$

$$\Delta G^\circ = \Delta H^\circ - T \Delta S^\circ \quad (9)$$

$$\ln K = \frac{\Delta S^\circ}{R} - \frac{\Delta H^\circ}{RT} \quad (10)$$

where R ($8.314 \text{ mol}^{-1} \text{K}^{-1}$) is the ideal gas constant, K is the equilibrium constant and T is the temperature at K .

2.2.4 Antimicrobial Study

2.2.4.1 Preparation and Standardization of Inoculum The bacterial strains were conformed for their purity and the colonies from the subculture plates were suspended in 10 mL of Luria Bertani (LB) broth (Tryptone 10.0 g, Yeast extract 5.0 g, NaCl 10.0 g in 1000 mL distilled water) and incubated at 37 °C for 18–24 h in an orbital shaker at 150 rpm to attain logarithmic phase culture. Following incubation, the turbidity of the test suspension was standardized to match 0.5 McFarland standard (corresponds to approximately 1.5×10^8 CFU/mL). The adjusted suspension was used as inoculum for lawn culture preparation within 15 min.

2.2.4.2 Preparation McFarland Nephelometer Standards [18] *Reagent A—(1%) Barium Chloride (BaCl₂)* Barium chloride (1%) was placed in 100 mL of volumetric flask followed by the addition of 50 mL of deionized water and mixed well to dissolve. The volume was made to 100 mL by addition of deionized water and stored in screw cap glass bottle at 25 °C.

Reagent B—(1%) Sulfuric Acid (H₂SO₄) To 90 mL of deionized water in volumetric flask 1 mL of concentrated sulfuric acid was slowly added. The volume was made to 100 mL by addition of deionized water and stored in screw cap glass bottle at 25 °C.

Preparation of 0.5 standard turbidity (Table 1).

2.2.4.3 Preparation of Lawn Culture Sterile Muller-Hinton Agar (MHA) (g/L) (Beef infusion: 300; Casein hydrolysate:

Table 1 McFarland standard turbidity solution ratio

Reagents/absorbance	McFarland standard tube no.				
	0.5	1	2	3	4
Barium chloride 1.0% (mL)	0.05	0.1	0.2	0.3	0.4
Sulfuric acid 1.0% (mL)	9.95	9.9	9.8	9.7	9.6
Approx. cell density (1×10^8 CFU/mL)	1.5	3.0	6.0	9.0	12.0
Transmittance% ^a	74.3	55.6	35.6	26.4	21.5
Absorbance ^a	0.08 to 0.1	0.257	0.451	0.582	0.669

^aAt wavelength of 600 nm

17.5; Starch: 1.5; Agar: 15; pH 7.2 ± 0.2) was prepared. The media was sterilized at 121°C at 15 lbs for 15 min. Diluted bacterial cultures adjusted to a 0.5 McFarland turbidity (1×10^8 CFU mL^{-1}) was spread evenly over the entire surface of the agar plates using sterile cotton swab. The plates were incubated for 15 min at room temperature. Using a well puncture 6–8 wells of 6 mm diameter were made for drug loading.

The antimicrobial activities of auto combusted ALW/CoFe₂O₄ were tested against *Staphylococcus aureus* (ATCC 25923); *Escherichia coli* (ATCC 25922) and *Candida albicans* (ATCC 10231) using well diffusion method on Mueller–Hinton agar plates. Disks with different concentration parameters of ALW/CoFe₂O₄ sonicated in distilled water were pipetted. The microorganisms were inoculated into nutrient broth medium, and incubated at 37°C for 2 to 5 h until it reached the turbidity of a 0.5 McFarland standard (0.05 mL of 1.175% BaCl₂·2H₂O with 9.95 mL of 1% H₂SO₄). Using a sterile swab they were cultured on a Mueller–Hinton agar plate. Disks with different concentrations of ALW/CoFe₂O₄ were placed on the surface of agar using forceps. After a period of pre-incubation (for 15 min), the inoculated plates were incubated at appropriate temperature for 24 h. The zone of inhibition was measured by Vernier caliper as a parameter of antibacterial property of the synthesized ALW/CoFe₂O₄. An additional media control plate

and antibiotic (Streptomycin) was also kept aside to monitor any contamination during testing.

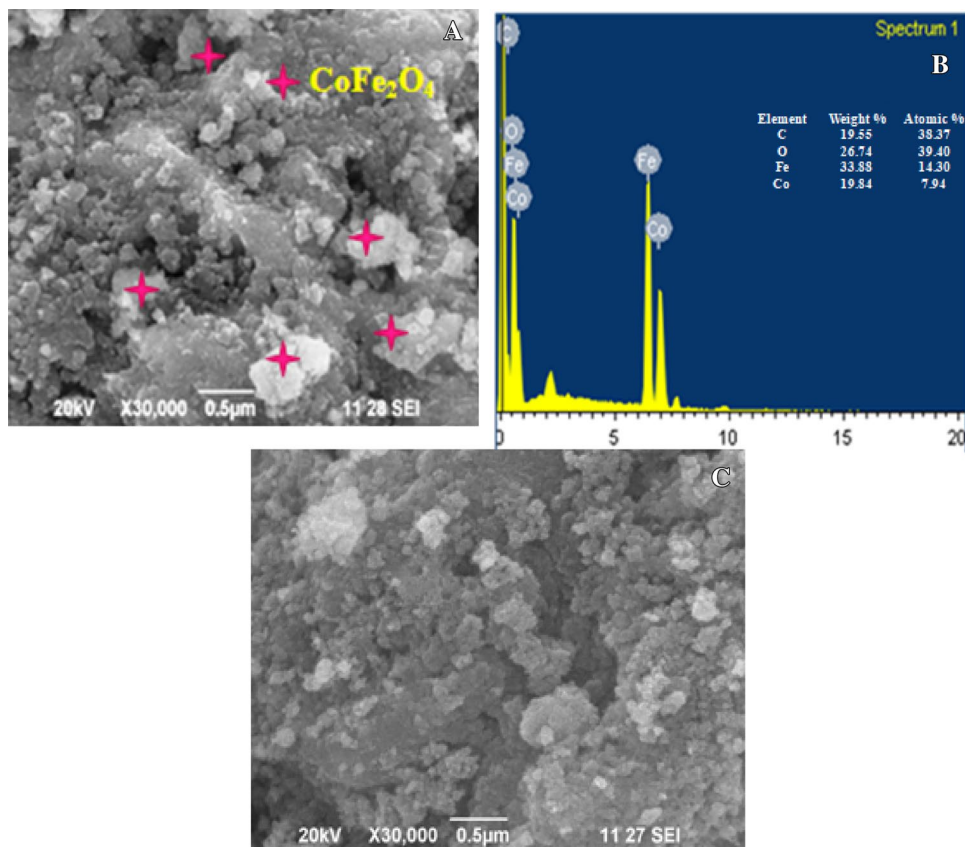
3 Results and Discussion

3.1 Characterization of Composite

Figure 1 shows the SEM image of ALW/CoFe₂O₄ and its respective EDAX spectra. As shown in Fig. 1a many spherical particles of CoFe₂O₄ are aggregated on the irregular shaped rough surface of ALW. This addition of CoFe₂O₄ which affects the morphology of ALW results high specific area. Such high specific area is conducive to adsorb RR141 molecules resulting in an improvement of adsorption efficiency. The corresponding EDAX spectra (Fig. 1b) clearly shows the presence of Co and Fe components in ALW/CoFe₂O₄. In addition, as can be seen from Fig. 1c, after RR141 loading to the surface of ALW/CoFe₂O₄, an active sites were occupied by the RR141 molecules.

Powder XRD can measure millions of crystals and accurately determine the size distribution which is the fundamental property of nanomaterials and can be widely used for studying the nature of polymers and composites in Material Science Fig. 2 shows the XRD patterns of ALW, pure CoFe₂O₄ and ALW/CoFe₂O₄ composite. The broad and low

Fig. 1 SEM morphology image before adsorption (a), after adsorption (c) and EDAX spectra (b) of ALW/CoFe₂O₄



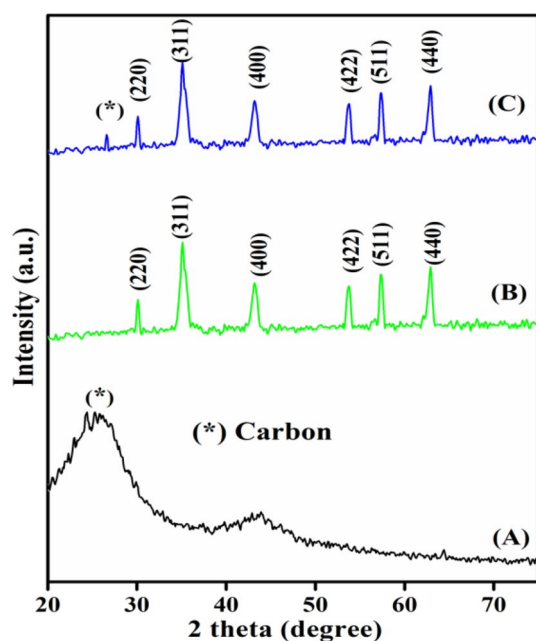


Fig. 2 XRD pattern of ALW (a), CoFe_2O_4 (b) and ALW/ CoFe_2O_4 (c)

diffraction peak at 25.8° in pattern (A) indicates the amorphous structure of ALW mentioned by *. The same peak (*) is observed in pattern (C) which is assigned to ALW/ CoFe_2O_4 . The diffraction peaks at 30° , 35.4° , 43.1° , 52.4° , 56.6° and 62.3° correspond to the crystal indices of (220), (311), (400), (422), (511), (440) confirm the spinel structure of CoFe_2O_4 which were well matched with the literature values (JCPDS Card No. 20-1086) [19]. The average crystalline size of nano particles (D) was estimated by using the Debye—Scherrer's equation [20].

$$D = \frac{0.9\lambda}{\beta \cos \theta} \quad (11)$$

where λ is X ray wave length, θ is Bragg diffraction angle and β is the full width. The estimated crystalline size of the synthesized nano particles is about 10 nm using FWHM of the peaks.

In general, the adsorption capacity increases with increasing specific surface area which governs the contact interfacial area that is available for adsorption [21]. The N_2 adsorption–desorption isotherms and the pore size distribution for ALW and ALW/ CoFe_2O_4 are shown in Fig. 3. The N_2 adsorption–desorption isotherms that exhibit the feature of type I curve with H4 hysteresis loop according to IUPAC indicate the presence of micro porous solids on the surface of ALW/ CoFe_2O_4 . The textural characteristics of ALW/ CoFe_2O_4 are presented in Table 2. The cobalt ferrite impregnation into ALW induced the decrease of BET surface area and the pore volume because the introduced CoFe_2O_4 was speculated to penetrate into the pores of ALW.

The lower surface area of ALW/ CoFe_2O_4 is due to the bigger weight contribution from CoFe_2O_4 on the surface of ALW. Even though the pores of ALW are blocked by cobalt ferrite nano particles, the average pore diameter of ALW/ CoFe_2O_4 (3.660 nm) is significantly higher to adsorb dye molecules. Furthermore, CoFe_2O_4 nano particles act as an activating agent due to the oxidation action of Fe for carbon based materials [22].

FTIR spectroscopy is an excellent tool for the identification of different groups due to the fact that each one represents different characteristic bands. It provides information on the basis of chemical composition and physical state of the whole sample. Figure 4 and Table 3 represent the FTIR spectra and assignments according to the observed spectral region of ALW and ALW/ CoFe_2O_4 nano composite. The broad absorption band of ALW between 3300 and 3500 cm^{-1} is related to stretching vibration of (O-H) hydroxyl group. The peak at 2362 cm^{-1} is characteristic to CH_2 bridges and C=O aliphatic ester group is observed at 1725 cm^{-1} . Moreover, the bands at 1661 cm^{-1} , 1585 cm^{-1} and 1220 cm^{-1} are assigned to aromatic C=C, CO stretching mode conjugated to NH deformation mode and C–OH stretching respectively. The new peaks at 1069 cm^{-1} and 585 cm^{-1} correspond to C–O stretching attributed to epoxy or alkoxy and the stretching vibration of Fe–O bond [23] respectively. These results demonstrate that CoFe_2O_4 is covalently bonded to the surface of ALW.

Thermal gravimetric analysis (TGA) is widely used to investigate the thermal decomposition of nano composite to determine the thermal decomposition kinetic parameter. These parameters can be used to obtain a better understanding of thermal stability of ALW/ CoFe_2O_4 . Figure 5 shows the TG and DSC curves ALW and ALW/ CoFe_2O_4 . Different weight loss were observed during heat treatment from room temperature to 600°C . At the beginning, the weight loss up to 140°C for ALW (A) was due to the removal of adsorbed water. After this, the weight loss till 320°C is attributed to the decomposition of oxygen containing functional groups. At the temperature range 100 – 350°C , two exothermic peaks are observed in DSC curves for the oxidative decomposition of carbon [23] and the weight of an activated carbon reduced to 11.18% is depicting to the pyrolysis of carbon. There is a slow and steady loss between the temperature 350 and 600°C . But this weight loss is greatly restricted in the curve of ALW/ CoFe_2O_4 (B) because of strong bonding of CoFe_2O_4 on ALW. This suggests that CoFe_2O_4 would increase the thermal stability and adsorptivity of ALW/ CoFe_2O_4 . Similar reports were observed for CoFe_2O_4 /activated carbon composite for the removal of Cr (VI) [5].

Figure 6 shows the magnetic hysteresis plot of ALW/ CoFe_2O_4 at room temperature. This field dependent magnetization curve shows the magnetic parameters such as saturation magnetization, negligible remanence and coercivity.

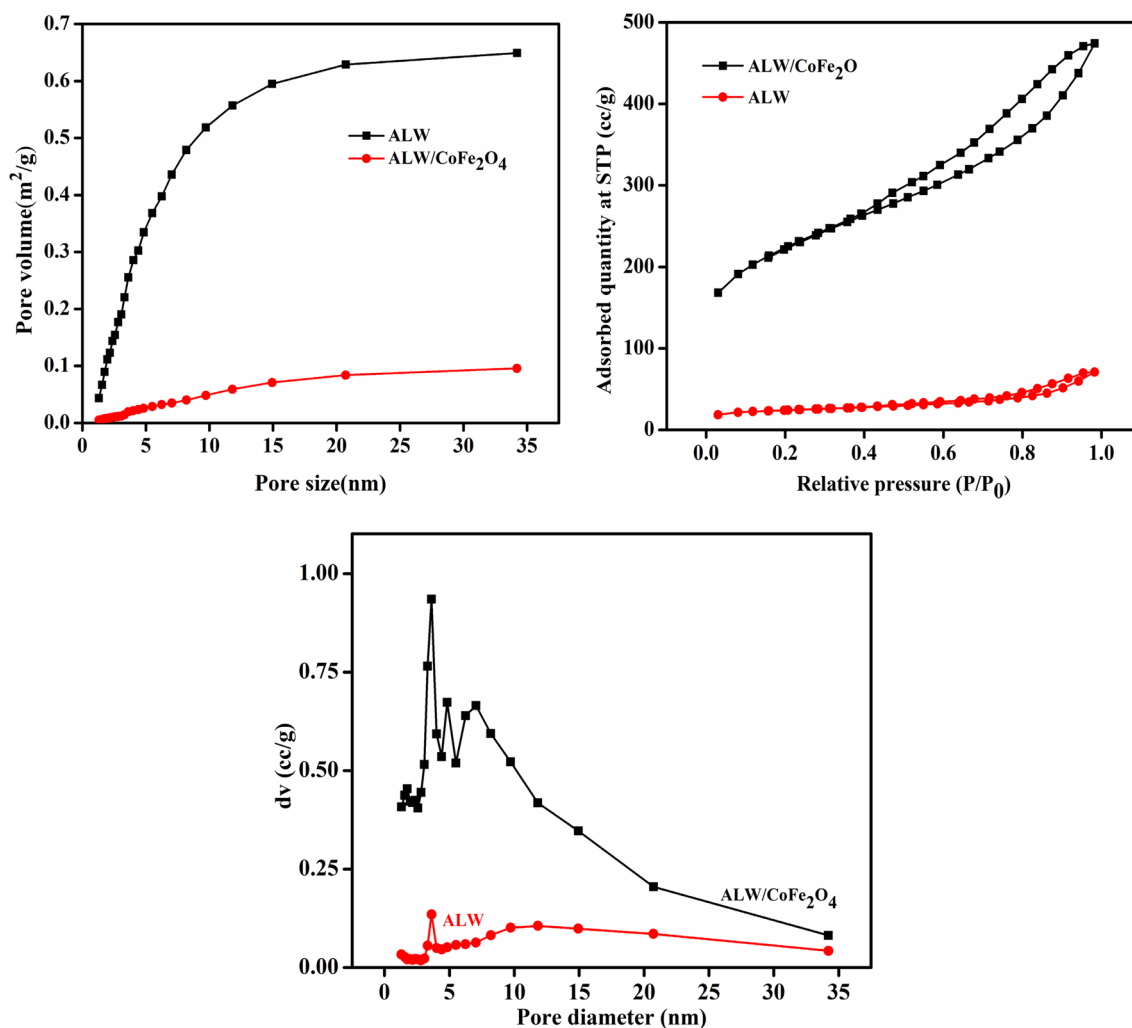


Fig. 3 N_2 adsorption/desorption isotherms and pore size distribution ALW and ALW/CoFe₂O₄

Table 2 Textural parameters obtained from N_2 adsorption–desorption isotherms

Samples	BET surface area (m ² /g)	Pore volume (cc/g)	Pore diameter (nm)
ALW	728.5	0.649	1.305
ALW/CoFe ₂ O ₄	77	0.096	3.660

These values indicate the ferromagnetic behavior of ALW/CoFe₂O₄. The saturation magnetization depends on particle size and encapsulation of ferrite nano particles with activated carbon which are confirmed by XRD patterns and SEM images respectively. The saturation magnetization value for ALW/CoFe₂O₄ was obtained as (M_s)—38.75 (emu/g) which is lower than pure CoFe₂O₄ (94 emu/g). The lower saturation magnetization value than pure CoFe₂O₄ is attributed to the attachment of CoFe₂O₄ with ALW, small

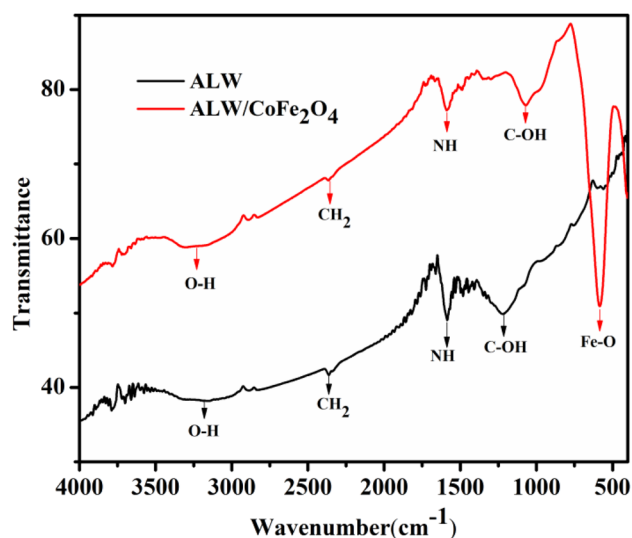
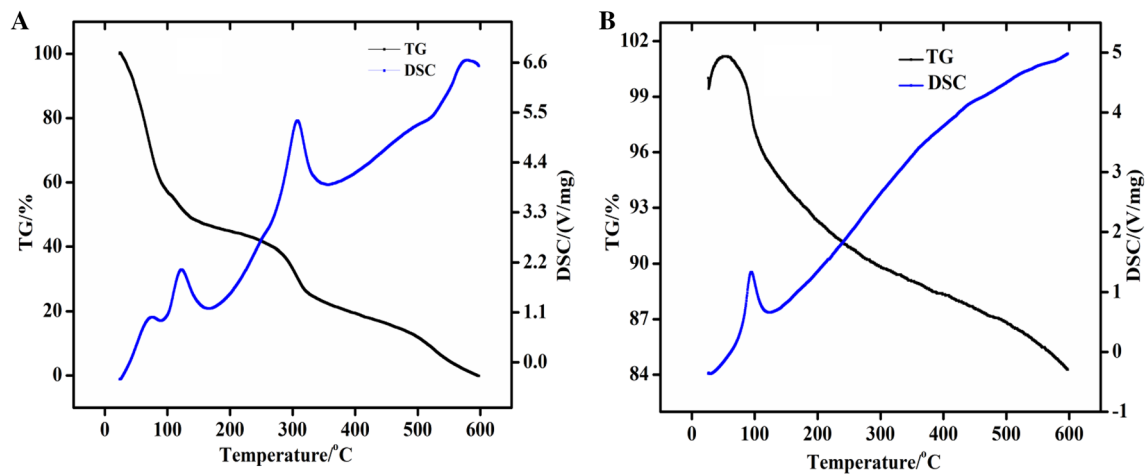
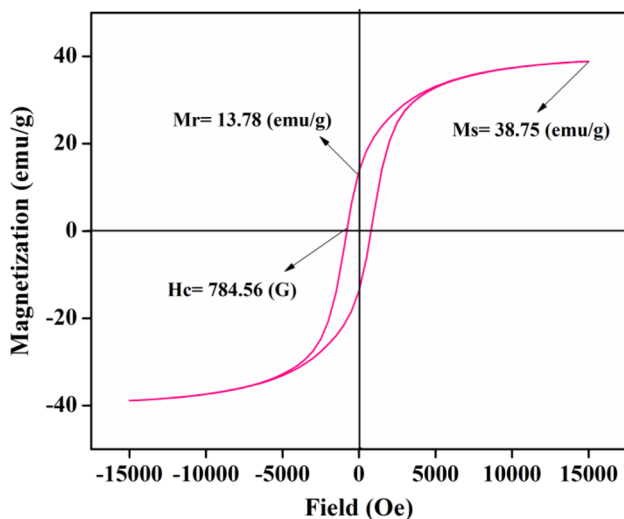


Fig. 4 FT-IR spectra of ALW and ALW/CoFe₂O₄

Table 3 FT-IR frequency assignments for ALW and ALW/CoFe₂O₄

Material	Frequency (cm ⁻¹)	Assignments
ALW	3300–3500	Stretching vibration of (O–H) [2]
	2362.37	CH ₂ bridges
	1725.01	C=O aliphatic ester group [24]
	1661.37	Aromatic C=C
	1585.2	CO stretching mode conjugated to NH deformation mode
	1220.72	C–OH stretching
ALW/CoFe ₂ O ₄	3300–3500	Stretching vibration of (O–H) [2]
	2362.37	CH ₂ bridges
	1725.01	C=O aliphatic ester group [24]
	1661.37	Aromatic C=C
	1585.2	CO stretching mode conjugated to NH deformation mode
	1220.72	C–OH stretching
	585.29	Stretching vibration of Fe–O [23]

**Fig. 5** TG and DSC curves of ALW (a) and ALW/CoFe₂O₄ (b)**Fig. 6** Magnetization curve of ALW/CoFe₂O₄

size and surface defect of CoFe₂O₄ crystallites. However, this magnetization is high enough to meet the needs of separation of nano composite after adsorption using an external magnet [25]. The negligible remanence and coercivity were also obtained as (M_r)—13.78 (emu/g) and (H_c)—784.56 (G) respectively. But the values of M_s , M_r and H_c are lower when compared with some other nano composites such as CoFe₂O₄/GO [20], CoFe₂O₄/Clinoptilolite [25] and CoFe₂O₄/AC [26].

3.2 Adsorption Study

3.2.1 Effect of Initial pH

The pH of the dye solution is an important parameter since the charge of the surface of the particles can affect the adsorption hence influencing the electrostatic interaction between the adsorbent and adsorbate. As the pH of the dye

molecules effect the degree of ionization and surface properties, that results the change of electrical affinity on the adsorbent [27]. The effect of initial pH on the adsorption of RR141 onto ALW/CoFe₂O₄ was investigated by varying pH between 3.0 and 12.0 using 0.1 N NaOH/HCl. As can be observed, at low pH, the removal efficiency of RR141 is higher than at high pH. At low pH, the positively charged surface of an adsorbent as a result of protonation process attract the negatively charged functional groups present in dye molecule. In a dye solution with higher pH values, the positive charge on the surface decreases and the displacement becomes difficult which results in a decrease in the efficiency of dye removal. Therefore, an increase in pH of solution does not favour the adsorption due to electrostatic repulsion. So the maximum removal was found to be at initial pH of 3 as seen in Fig. 7.

3.2.2 Effect of Adsorbent Dosage

Figure 8 shows the effect of dosage of ALW/CoFe₂O₄ on RR141 removal. This study of effect of adsorbent dosage was observed by varying the amount of composite from 25 to 250 mg with initial dye concentration of 50 mg/L, pH of 6.5, temperature of 30 °C and an agitation time of 70 min. According to this, the percent removal of dye is increased with increase in composite dosage and attained a plateau after a particular dose for all the concentrations of the dye. This result is due to the increase of the surface area consequent to the increase in the number of particles with more number of active sites for adsorption and saturation occurs as a result of non availability of dye molecules. This may also be due to the increase in effective surface area resulting

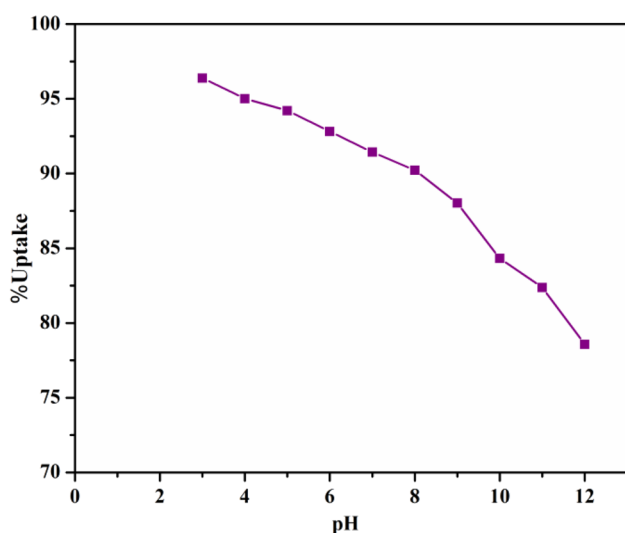


Fig. 7 Effect of initial solution pH on RR141 adsorption of ALW/CoFe₂O₄

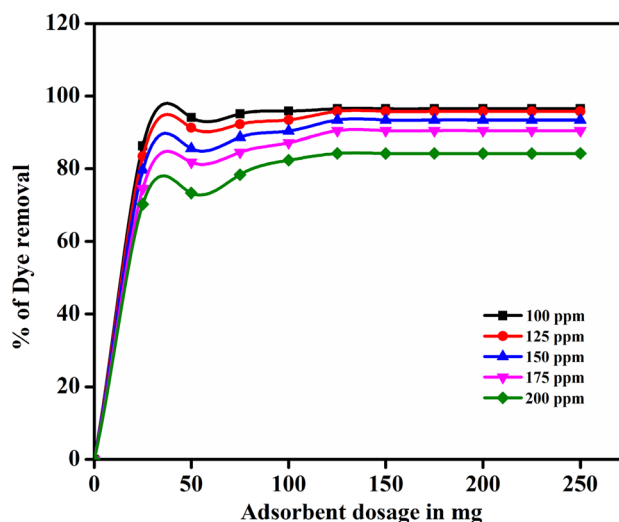


Fig. 8 Effect of adsorbent dosage on RR141 adsorption of ALW/CoFe₂O₄

from the conglomeration of the adsorbent especially at higher dosage of the adsorbent.

3.2.3 Effect of Contact Time and Initial Dye Concentration with Adsorption Kinetics and Isotherms

The adsorption capacity of an adsorbent by the distribution of the dye molecules on the surface of adsorbent is based on contact time which is to be needed to attain an equilibrium. The equilibrium attainments of the mesoporous activated carbons with smaller particle size are greater than the microporous carbons. The effect of contact time was carried out at constant initial dye concentration, temperature and pH with suitable adsorbent dosage. The results indicate that the removal of dye is increased progressively with contact time and attained saturation after equilibrium time. The rate of adsorption was higher in the initial stages because of the availability of active binding sites for dye molecules, which become saturated with time resulting in lower adsorption rate [24]. Also, the percent removal is decreased with the increase in dye concentration but the amount of dye adsorbed is increased suggesting that the dye removal is concentration dependent. The optimum time was considered to be 70 min for RR141 adsorption onto ALW/CoFe₂O₄ and the results are shown in Fig. 9. The curves are found to be single, smooth and continuous leading to saturation indicating the possibilities of formation of monolayer coverage of dye on the outer surface of an adsorbent [28].

The experimental data were analyzed initially with the pseudo first-order kinetic model and then with pseudo second order kinetic model. Figure 9b represents the plot of $\log(q_e - q_t)$ versus t that gives the linear relationship from which k_1 and q_e can be determined by the slope of $-\frac{k_1}{2.303}$ and

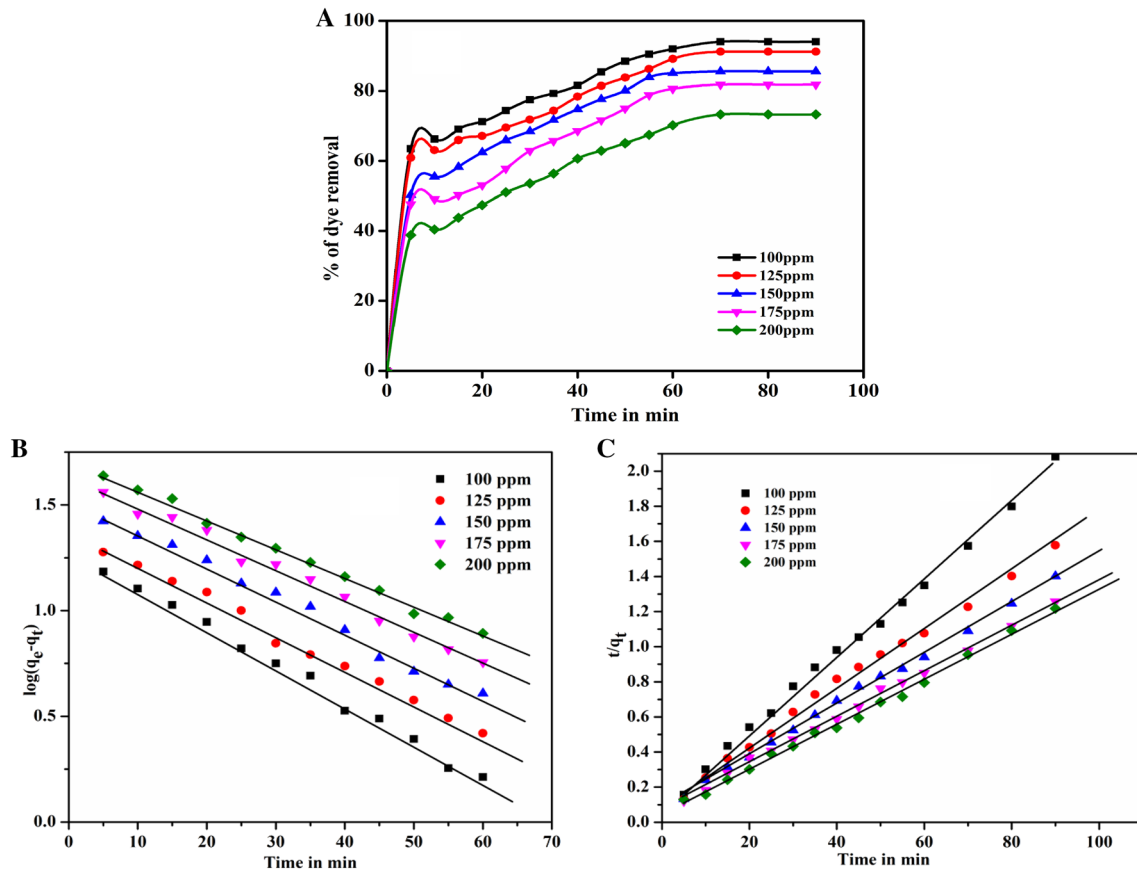


Fig. 9 a Effect of agitation time with initial dye concentration, b pseudo first order kinetic plot and c pseudo second order kinetic plot on RR141 adsorption of ALW/CoFe₂O₄

intercept of $\log q_e$, respectively. The results indicate that R^2 values for pseudo first order kinetic model are relatively lower and the calculated $q_e(\text{cal})$ values are significantly varied from experimental values. So, further the experimental data were fitted with the second-order kinetic model. Figure 9c shows linear plots of t/q_t vs t with a slope of $1/q_e$ and an intercept of $\frac{1}{k_2 q_e^2}$. The plots are found to be linear with good correlation coefficients. The theoretical $q_e(\text{cal})$ values are well agreed with $q_e(\text{exp})$ values at all the studied conditions and R^2 values are also high, which indicate the

applicability of pseudo second order to describe an adsorption process. This implies that the second-order model is in good agreement with the experimental data and can be used to favorably explain an adsorption of RR141 on ALW/CoFe₂O₄. The results conclude that the second order kinetics equation is the best fitting kinetic model (Table 4).

The equilibrium data for adsorption of RR141 onto ALW/CoFe₂O₄ was modeled using Langmuir and Freundlich isotherms. According to the Langmuir model, the slope and intercept of linear plot (Fig. 10a) of C_e versus C_e/q_e yield the values of q_m and K_L respectively and the R_L value was found

Table 4 Adsorption kinetic parameters of RR141 on ALW/CoFe₂O₄ composite

Conc (mg/L)	$q_e(\text{exp})$ (mg/g)	Pseudo first order			Pseudo second order		
		k_1 (min ⁻¹)	$q_e(\text{cal})$ (mg/g)	R^2	$k_2 \times 10^{-3}$ (min ⁻¹)	$q_e(\text{cal})$ (mg/g)	R^2
100	47.06	0.041	19.5	0.995	0.20	47.62	0.997
125	57.03	0.037	23.6	0.994	0.42	62.5	0.994
150	64.21	0.034	33.88	0.990	0.45	71.43	0.998
175	71.59	0.032	43.85	0.990	0.43	83.33	0.997
200	73.28	0.029	50.93	0.995	0.31	83.33	0.996

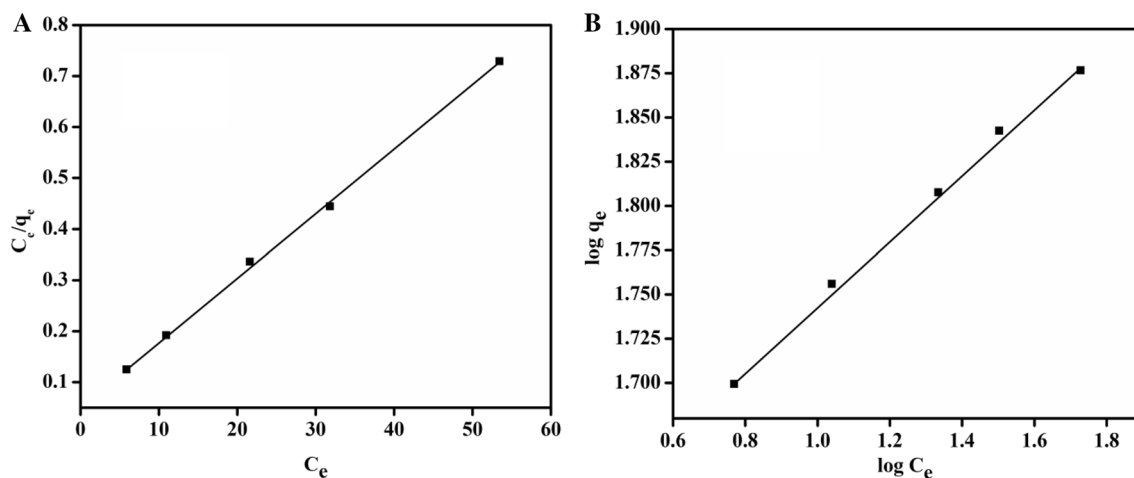


Fig. 10 **a** Langmuir isotherm, **b** Freundlich isotherm on RR141 adsorption of ALW/CoFe₂O₄

to be between 0 and 1. The constants K_F and $1/n$ which represent the adsorption capacity and adsorption intensity respectively are obtained from intercept and slope of linear regression plot (Fig. 10b) of Freundlich isotherm model. The isotherm constants and correlation coefficients from two models are listed in Table 5. As can be seen from results, the maximum adsorption capacity q_m is 83.33 mg/g and the correlation coefficient (R^2) from Langmuir isotherm is significantly greater than Freundlich isotherm. The fact that the experimental data is better modeled with Langmuir isotherm represents the specific number of sites on the surface of adsorbent where the adsorbate molecules can be adsorbed and also involve the monolayer adsorption with no lateral interaction between the adsorbed molecules [29].

3.2.4 Effect of Temperature and Adsorption Thermodynamics

The adsorption experiments were carried out at various temperatures of 30 °C, 40 °C, 50 °C and 60 °C under optimized conditions. Figure 11a depicts the effect of temperature on ALW/CoFe₂O₄ for RR141 removal. The percentage removal of RR141 increased with increase in temperature. With increasing temperatures, the adsorption capacity increased from 47.0 to 58.37 mg/g. The standard enthalpy (ΔH°), standard entropy (ΔS°) and standard free energy (ΔG°) were estimated and applied in Van't Hoff equation. The values of ΔS° and ΔH° were obtained from slope and intercept of Van't Hoff plot (Fig. 11b) of $\ln K$ vs $1/T$. The values of ΔS° ,

ΔH° and ΔG° are listed in Table 6. The more negative ΔG° indicates that the adsorption favor higher temperature. The negative values of ΔG° and ΔH° indicate the spontaneity and exothermic nature of adsorption. The positive value of ΔS° reflects the increased randomness at the solid–liquid interface.

3.3 Antimicrobial Activity

The antimicrobial activity of ALW/CoFe₂O₄ was carried out against *Staphylococcus aureus*, *Escherichia coli* and *Candida albicans* using well diffusion method. The antimicrobial property with different concentrations (100–500 mg) was ascertained by determination of the clear zone of inhibition around the disc after 48-h incubation and the obtained results are presented in (Table 7; Fig. 13, show the bar diagram for the Zone of Inhibition values for comparison). The antimicrobial activity was compared with commercial antimicrobial agent—Streptomycin and Amphotericin B, as a positive control impregnated on the disc. The antibacterial and fungistatic effect of ALW/CoFe₂O₄ against *S. aureus* and *C. albicans* were more or less same in the range between 11 and 17.56 mm of zone of inhibition than in *E. coli*. The mechanism of antimicrobial activity for the nanoparticles is may be due to : (1) interference during cell wall synthesis; (2) suppression during protein biosynthesis (translation); (3) interference or disruption of transcription process; and (4) disruption of primary metabolic pathways [11].

Table 5 Isotherm constants for adsorption on ALW/CoFe₂O₄

Langmuir isotherm				Freundlich isotherm		
q_m (mg/g)	K_L (L/mg)	R^2	R_L	K_F [mg/g(mg L ⁻¹)] ^{-1/n}	N	R^2
83.33	0.226	0.999	0.0652	36.31	5.41	0.998

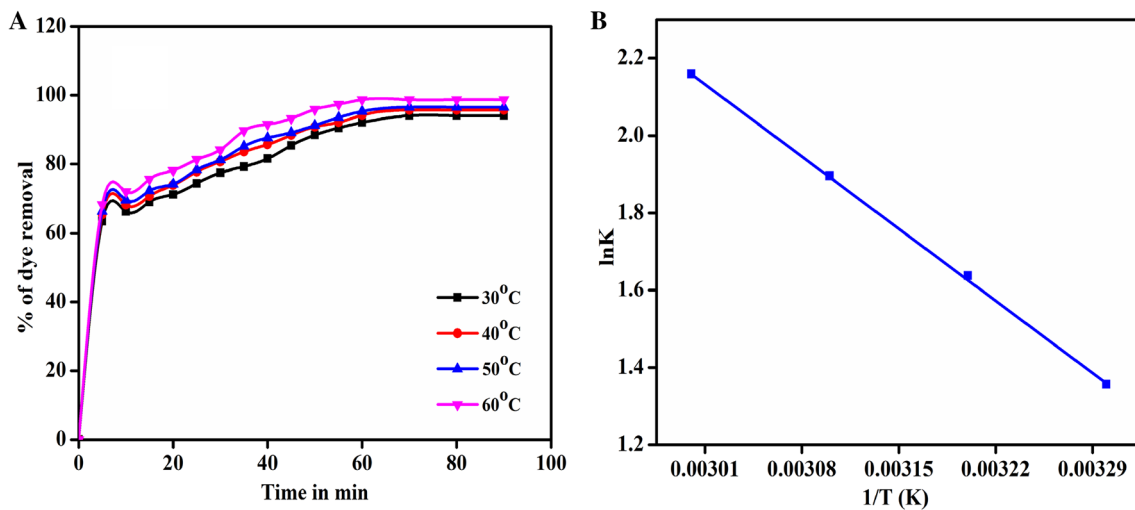


Fig. 11 a Effect of temperature, b Van't Hoff plot on RR141 adsorption of ALW/CoFe₂O₄

Table 6 Thermodynamic parameters for adsorption of RR141 on ALW/CoFe₂O₄

ΔS° (KJ/mol)	ΔH° (KJ/mol)	ΔG° (KJ/mol)			
		30 °C	40 °C	50 °C	60 °C
74.052	18.365	-3218.48	-4061.53	-5191.54	-5677.38

Table 7 Inhibitory activity of ALW/CoFe₂O₄

Sample name	Concentration in mg/L	Zone of inhibition in mm		
		<i>E.coli</i>	<i>S.aureus</i>	<i>C.albicans</i>
ALW/CoFe ₂ O ₄	100	10.5 ± 0.40	11.83 ± 0.23	11.0 ± 0.24
	200	10.83 ± 0.23	14.0 ± 0.41	12.1 ± 0.14
	300	12.5 ± 0.41	15.75 ± 0.20	14.16 ± 0.23
	400	15.33 ± 0.24	16.33 ± 0.23	17.33 ± 0.33
	500	17.0 ± 0.41	17.5 ± 0.16	17.6 ± 0.08
Streptomycin/amphotericin B	10	19.0 ± 0.41	19.16 ± 0.23	27.96 ± 0.04

The antimicrobial potency of ALW/CoFe₂O₄ is through electrostatic interaction of metal nano particles and the surface of microbes producing oxidative stress and DNA damage which leads to impaired membrane function. The inactivation of bacterial enzymes by Co ions present in nano clusters results in cell death [30]. Figure 12a indicates the inhibitory activity of ALW/CoFe₂O₄ against the bacteria *Staphylococcus aureus* and *Escherichia coli*, (b) represents anti fungal activity against *Candida albicans* and this antimicrobial activity is compared with standard Streptomycin.

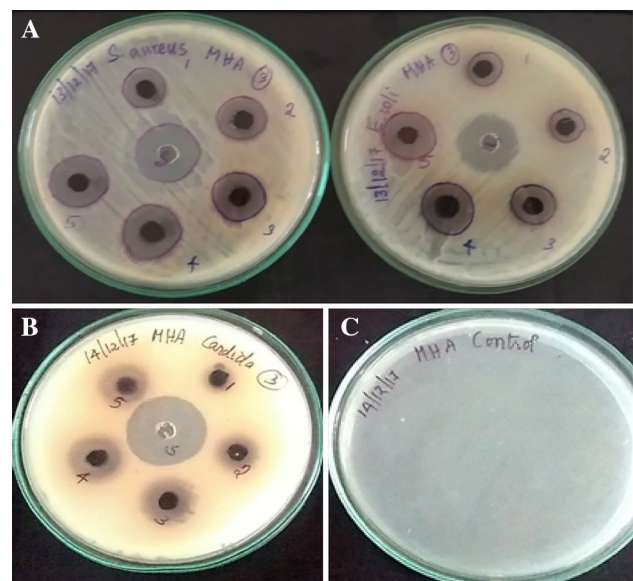


Fig. 12 Inhibitory activity of ALW/CoFe₂O₄ against a *Staphylococcus aureus*, *Escherichia coli*, b *Candida albicans*, c Streptomycin/Amphotericin (standard)

4 Conclusion

In summary, we have fabricated magnetic ALW/CoFe₂O₄ nano composite by a facile auto combustion method for the removal of RR141 from aqueous solution. The SEM with EDAX, XRD and IR showed the encapsulation of CoFe₂O₄ nano particles into the pores of ALW activated carbon which provided the spinel structured ALW/CoFe₂O₄. The BET surface area of ALW/CoFe₂O₄

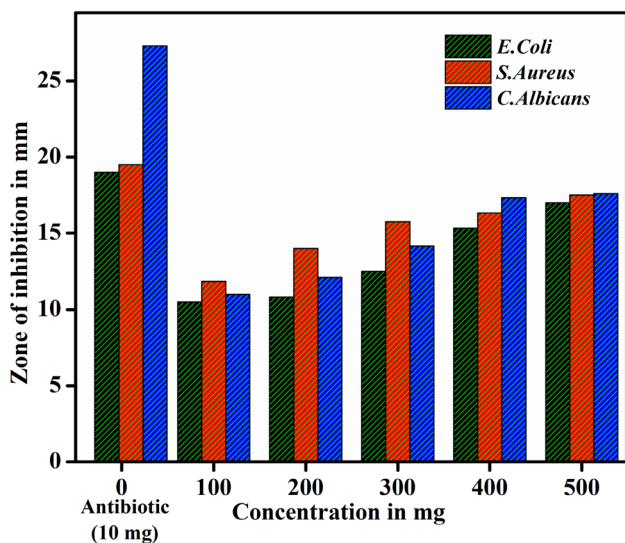


Fig. 13 Bar diagram for the Zone of Inhibition values

was lower than ALW activated carbon indicated that the micro pores of AC are filled with CoFe_2O_4 nanoparticles. However, an adsorption of RR141 on ALW/ CoFe_2O_4 was effective by the oxidation action of Fe in CoFe_2O_4 . The magnetic property of ALW/ CoFe_2O_4 by VSM provided an efficient way to separate it easily from the solution with the help of an external magnetic field, which is very useful in the removal of pollutants from a large volume of aqueous solution. Subsequently, prepared adsorbent was successfully applied for the removal of RR141 from aqueous solutions. The process parameters such as pH, adsorbent dose, equilibrium contact time, initial dye concentration and temperature were optimized. The predicted optimum conditions for maximum removal (94.12%) were estimated to be 100 mg/L initial concentration, pH 6.5, 50 mg dose and 70 min contact time. The kinetics of the adsorption followed pseudo-second order model which indicated the chemical nature of adsorption. Whereas, the isotherm characteristics have been fitted well with the Langmuir equation. The maximum Langmuir adsorption capacity for RR141 removal on ALW/ CoFe_2O_4 was found to be 83.33 mg/g. Thermodynamic parameters (ΔS° , ΔH° and ΔG°) indicate the adsorption to be spontaneous, endothermic and accompanied with increase in randomness. Furthermore, antimicrobial activity of ALW/ CoFe_2O_4 was studied against *Staphylococcus aureus*, *Escherichia coli*, *Candida albicans* and compared with standard *Streptomyces*. Thus it is concluded that, ALW/ CoFe_2O_4 is promising derived sorbent due to its nano size and magnetic property resulting in the greater adsorption capacity and also antimicrobial activity.

References

- M. Goswami, P. Phukan, Enhanced adsorption of cationic dyes using sulfonic acid modified activated carbon. *Environ. Chem. Eng.* **5**, 3508–3517 (2017)
- J. Sukriti, A.S. Chadha, V. Pruthi, P. Anand, J. Bhatia, B.S. Kaith, Sequestration of dyes from artificially prepared textile effluent using RSM-CCD optimized hybrid backbone based adsorbent-kinetic and equilibrium studies. *J. Environ. Manag.* **190**, 176–187 (2017)
- C. Palma, L. Lloret, A. Puen, M. Tobar, E. Contrerasb, Production of carbonaceous material from avocado peel for its application as alternative adsorbent for dyes removal. *Chin. J. Chem. Eng.* **24**, 521–528 (2016)
- S. Yavaria, N.M. Mahmoodib, P. Teymouria, B. Shahmoradia, A. Malekia, Cobalt ferrite nanoparticles: preparation, characterization and anionic dye removal capability. *J. Taiwan Inst. Chem. Eng.* **59**, 320–329 (2016)
- W. Qiu, D. Yang, J. Xu, B. Hang, H. Jin, D. Jin, X. Peng, J. Li, H. Ge, X. Wona, Efficient removal of Cr (VI) by magnetically separable CoFe_2O_4 /activated carbon composite. *J. Alloys Compd.* **678**, 179–184 (2016)
- K. Kombaiah, J.J. Vijaya, L.J. Kennedy, M. Bououdina, R.J. Ramalingam, H.A. Al-Lohedan, Okra extract-assisted green synthesis of CoFe_2O_4 nanoparticles and their optical, magnetic and antimicrobial properties. *Mater. Chem. Phys.* **204**, 410–419 (2018)
- F. Huixia, C. Baiyi, Z. Deyi, Z. Jianqiang, T. Lin, Preparation and characterization of the cobalt ferrite nano-particles by reverse coprecipitation. *J. Magn. Magn. Mater.* **356**, 68–72 (2014)
- F. Dehghani, S. Hashemian, A. Shibani, Effect of calcination temperature for capability of MFe_2O_4 ($\text{M} = \text{Co}, \text{Ni}_2$ and Zn) ferrite spinel for adsorption of bromophenol red. *J. Ind. Eng. Chem.* **48**, 36–42 (2017)
- A. Almasian, F. Najafi, M. Mirjalili, M.P. Gashti, G.C. Fard, Zwitter ionic modification of cobalt-ferrite nanofiber for the removal of anionic and cationic dyes. *J. Taiwan Inst. Chem. Eng.* **67**, 306–317 (2016)
- D.H.K. Reddy, Y.-S. Yuna, Spinel ferrite magnetic adsorbents: alternative future materials for water purification? *Coord. Chem. Rev.* **315**, 90–111 (2016)
- C.H.S. Chakra, K.V. Rao, T. Pavani, Antimicrobial activity of pure Cu nano particles synthesized by surfactant varied chemical reduction method. *Environ. Nanotechnol. Monit. Manag.* **6**, 88–94 (2016)
- R. Žalneravičius, A. Paškevičius, M. Kurtinaitiene, A. Jagminas, Size-dependent antimicrobial properties of the cobalt ferrite nanoparticles. *J. Nanopart. Res.* **18**, 1–10 (2016)
- N. Sanpo, C.C. Berndt, C. Wen, J. Wang, Transition metal substituted cobalt ferrite nano particles for biomedical applications. *Acta Biomater.* **9**, 5830–5837 (2013)
- A.H. Ashour, A.I. El-Batal, M.I.A. Abdel Maksoud, G.S. El-Sayyad, S. Labib, E. Abdeltwab, N.M. El-okr, Antimicrobial activity of metal substituted cobalt ferrite nanoparticles synthesized by sol-gel technique. *Particuology* **48**, 141–151 (2018)
- M.I.A. Abdel Maksoud, G.S. El-Sayyad, A.H. Ashour, A.I. El-Batal, M.S. Abd-Elmonem, H.A.M. Hendawy, E.K. Abdel-Khalek, S. Labib, E. Abdeltwab, M.M. El-Okr, Synthesis and characterization of metals-substituted cobalt ferrite [$\text{M}_x\text{Co}(1-x)\text{Fe}_2\text{O}_4$; ($\text{M} = \text{Zn}, \text{Cu}, \text{Mn}$; $x = 0, 0.5$) nanoparticles as antimicrobial agents and sensors for Anagrelide determination in biological samples. *Mater. Sci. Eng. C* **1**, 644–656 (2018)
- K. Karthik, C.P. Saraswathy, Antimicrobial activity of chemically modified activated carbon of tribulus terrestris. *Res. Biotechnol.* **6**, 42–46 (2015)

17. T.K.M.P. Kumar, T.R. Mandlimath, P. Sangeetha, P. Sakthivel, S.K. Revathi, S.K. Ashok Kumar, S.K. Sahoo, Highly efficient performance of activated carbon impregnated with Ag, ZnO and Ag/ZnO nanoparticles as antimicrobial materials. *RSC Adv.* **5**, 108034–108043 (2015)
18. K.C. Chapin, T. Lauderdale, Reagents, stains, and media: bacteriology, in *Manual of Clinical Microbiology*, 8th edn., ed. by P.R. Murray, E.J. Baron, J.H. Jorgensen, M.A. Pfaller, R.H. Tenover (ASM Press, Washington, DC, 2003), p. 358
19. E.R. Kumar, R. Jayaprakash, T.A. Kumar, S. Kumar, Effect of reaction time on particle size and dielectric properties of manganese substituted CoFe_2O_4 nano particles. *J. Phys. Chem. Solid* **74**, 110–114 (2013)
20. T. Prakash, R. Jayaprakash, G. Neri, A comparative study of the synthesis of CdO nanoplatelets by an albumen-assisted isothermal evaporation method. *J. Alloys Compd.* **624**, 258–265 (2015)
21. D. Chen, Z.Y. Zeng, Y. Zeng, F. Zhang, M. Wang, Removal of methylene blue and mechanism on magnetic $\gamma\text{-Fe}_2\text{O}_3/\text{SiO}_2$ nano composite from aqueous solution. *Water Resour. Ind.* **15**, 1–13 (2016)
22. M.H. Do, N.H. Phan, T.D. Nguyen, T.T.S. Phan, V.K. Nguyen, T.T. Trang, T.K.P. Nguyen, Activated carbon/ Fe_3O_4 nanoparticle composite: fabrication, methyl orange removal and regeneration by hydrogen peroxide. *Chemosphere* **85**, 1269–1276 (2011)
23. G. Wang, Y. Ma, Z. Wei, M. Qi., Development of multifunctional cobalt ferrite/graphene oxide nanocomposites for magnetic resonance imaging and controlled drug delivery. *Chem. Eng. J.* **289**, 150–160 (2016)
24. T.A. Khan, R. Rahman, E.A. Khan, Decolorization of bismarck brown R and crystal violet in liquid phase using modified pea peels: non-linear isotherm and kinetics modeling. *Model. Earth Syst. Environ.* **2**, 1–11 (2016)
25. Y. Huang, W. Wang, Q. Feng, F. Dong, Preparation of magnetic clinoptilolite/ CoFe_2O_4 composites for removal of Sr^{2+} from aqueous solutions: kinetic, equilibrium and thermodynamic studies. *J. Saudi Chem. Soc.* **21**, 58–66 (2017)
26. S. Sheshmani, B. Falahat, F.R. Nikmaram, Preparation of magnetic graphene oxide-ferrite nanocomposites for oxidative decomposition of Remazol Black B. *Int. J. Biol. Macromol* **97**, 671–678 (2017)
27. E. Altıntığ, H. Altundag, M. Tuzen, A. Saric, Effective removal of methylene blue from aqueous solutions using magnetic loaded activated carbon as novel adsorbent. *Chem. Eng. Res. Des.* **122**, 151–163 (2017)
28. I.D. Mall, V.C. Srivastava, N.K. Agarwal, I.M. Mishra, Removal of congo red from solution by bagasse fly ash and activated carbon: kinetic study and equilibrium isotherm analyses. *Chemosphere* **61**, 492–501 (2005)
29. R. Kamaraj, P. Ganesan, J. Lakshmi, S. Vasudevan, Removal of copper from water by electro coagulation process—effect of alternating current (AC) and direct current (DC). *Environ. Sci. Pollut. Res.* **20**, 399–412 (2013)
30. N.S. Alahmadi, J.W. Betts, F. Cheng, M.G. Francesconi, S.M. Kelly, A. Kornherr, T.J. Prior, J.D. Wadhawan, Synthesis and antibacterial effects of cobalt–cellulose magnetic nanocomposites. *RSC Adv.* **7**, 20020–20026 (2017)